AJNR

**Normal appearance of arachnoid granulations on contrast-enhanced CT and MR of the brain: differentiation from dural sinus disease.**

J L Leach, B V Jones, T A Tomsick, C A Stewart and M G Balko

This information is current as of June 3, 2025.

# Normal Appearance of Arachnoid Granulations on Contrast-Enhanced CT and MR of the Brain: Differentiation from Dural Sinus Disease

James L. Leach, Blaise V. Jones, Thomas A. Tomsick, Cheryl A. Stewart, and M. Gregory Balko

**PURPOSE:** To determine the imaging appearance and frequency with which arachnoid granulations are seen on contrast-enhanced CT and MR studies of the brain. **METHODS:** We retrospectively reviewed 573 contrast-enhanced CT scans and 100 contrast-enhanced MR studies of the brain for the presence of discrete filling defects within the venous sinuses. An anatomic study of the dural sinuses of 29 cadavers was performed, and the location, appearance, and histologic findings of focal protrusions into the dural sinus lumen (arachnoid granulations) were assessed and compared with the imaging findings. **RESULTS:** Discrete filling defects within the dural sinuses were found on 138 (24%) of the contrast-enhanced CT examinations. A total of 168 defects were found, the majority (92%) within the transverse sinuses. One third were isodense and two thirds were hypodense relative to brain parenchyma. Patients with filling defects were older than patients without filling defects (mean age, 46 years versus 40 years). Discrete intrasinus signal foci were noted on 13 (13%) of the contrast-enhanced MR studies. The foci followed the same distribution as the filling defects seen on CT scans and were isointense to hypointense on T1-weighted images, variable in signal on balanced images, and hyperintense on T2-weighted images. Transverse sinus arachnoid granulations were noted adjacent to venous entrance sites in 62% and 85% of the CT and MR examinations, respectively. Arachnoid granulations were found in 19 (66%) of the cadaveric specimens, in a similar distribution as that seen on the imaging studies. **CONCLUSION:** Discrete filling defects, consistent with arachnoid granulations, may be seen in the dural sinuses on 24% of contrast-enhanced CT scans and on 13% of MR studies. They are focal, well-defined, and typically located within the lateral transverse sinuses adjacent to venous entrance sites. They should not be mistaken for sinus thrombosis or intrasinus tumor, but recognized as normal structures.

Index terms: Arachnoid, anatomy; Brain, anatomy; Dural sinuses

Normal variations in cerebral venous anatomy are commonly encountered when interpreting imaging studies and may cause diagnostic confusion, especially relating to sinus thrombosis (1–3). One sign of thrombosis is diminished luminal contrast opacification of the dural sinus on computed tomographic (CT) and magnetic resonance (MR) imaging studies (2, 4–6). Nonpathologic processes have also been described that can produce a similar appearance. These include high or asymmetric superior sagittal sinus bifurcation (3); intrasinus septa, fenestrations, and duplications (7); and delayed scanning after contrast administration (8). Arachnoid granulations protruding into the sinus lumen may produce a focal filling defect in the contrast column on angiograms and CT scans and signal foci within the sinus lumen on MR images that can simulate focal thrombosis or tumor (1, 2, 9–12). Previous authors (12) have stated that the frequency with which apparent arachnoid granulations are seen on imaging studies is between 0.3 and 1 in 100 adults. Our experience indicates that they may be seen more frequently. Documentation of the

appearance, distribution, and frequency of occurrence of these normal structures is needed to prevent the erroneous diagnosis of venous sinus disease.

## Materials and Methods

### Imaging Evaluation

We randomly selected and evaluated 573 contrast-enhanced CT studies of the brain obtained at our institution between 1992 and 1994. Patients with a known history of dural sinus thrombosis, traumatic or surgical sinus disruption, or whose imaging studies were technologically inadequate were excluded from analysis.

CT was performed by using 3- to 5-mm collimation through the posterior fossa, followed by 10-mm contiguous scans through the remainder of the brain. Iodinated contrast material (150 mL iohexol or iothalamate meglumine) was administered by rapid infusion (50 mL by intravenous bolus followed with 100 mL by rapid drip infusion) during scanning. All scans were evaluated at a window level of +50; window widths of 200 Hounsfield units (HU) were used through the lower posterior fossa, 150 HU through the middle and upper posterior fossa (upper brain stem), and 100 HU through the reminder of the brain. The transverse sinuses, sigmoid sinuses, and torcular Herophili were visible on images with window widths of 150 or 200 HU. The location (superior sagittal sinus, torcular Herophili, medial transverse sinus, middle to lateral transverse sinus, transverse sinus–sigmoid sinus junction, or sigmoid sinus), density relative to brain, linear distance from the torcular Herophili, and size of any focal filling defect within the dural sinuses were recorded. To exclude pseudodefects from partial volume averaging of adjacent brain, only those defects that were well defined and round and had luminal contrast surrounding more than 50% of their circumference were counted. Because of the axial scan plane of CT, the proximal (horizontal) portion of the superior sagittal sinus was poorly seen, and evaluation of this region could not be made accurately. MR examinations were available in 31 of the 138 cases with filling defects and were correlated with findings on CT scans.

MR examinations were performed on 1.5- and 1.0-T scanners. Standard spin-echo T1-weighted (500–640/10/2 [repetition time/echo time/excitations]), proton density–weighted (2000–3000/20–30/1–2), and T2-weighted (2000–3000/80–100/1–2) images were obtained followed by axial and coronal T1-weighted acquisitions after intravenous administration of contrast material (0.1 mmol/kg). Images were 5 to 6 mm thick, with a 1-mm intersection gap.

After the MR appearance of the filling defects had been determined by comparing the CT and MR findings, we evaluated an additional 100 randomly selected contrast-enhanced MR studies.

Well-defined focal areas of nonflow signal projecting into the sinus lumen on MR images were recorded. Strin-

**TABLE 1: Distribution of 168 focal filling defects within the dural venous sinuses in 573 randomly selected contrast-enhanced CT examinations of the brain**

| Defect Location | n (%) |
|---|---|
| Right transverse sinus | 66 (39) |
|   Transverse/sigmoid junction | 4 (2) |
|   Midlateral transverse | 58 (35) |
|   Medial transverse near torcula | 4 (2) |
| Left transverse sinus | 88 (52) |
|   Transverse/sigmoid junction | 13 (8) |
|   Midlateral transverse | 71 (42) |
|   Medial transverse near torcula | 4 (2) |
| Sigmoid sinus | 3 (2) |
|   Left | 1 (0.6) |
|   Right | 2 (1) |
| Torcular Herophili | 8 (5) |
| Distal superior sagittal sinus | 1 (0.6) |
| Straight sinus | 2 (1) |

gent criteria were followed in order to eliminate areas of signal caused by complex, turbulent, or slow flow. These criteria included definite intrasinus position, visibility on all pulse sequences and imaging planes, and contrast surrounding more than 50% of the circumference of the defect. The defect's signal, size, and linear distance from the midline were recorded.

### Anatomic Evaluation

The dural sinuses (distal superior sagittal sinus, transverse sinus, sigmoid sinus, and straight sinus) were carefully dissected and examined in 29 cadavers. The age range of the cadavers was 41 to 91 years (mean, 69 years); eight were female and 20 were male. Because of the lack of imaging studies depicting apparent arachnoid granulations in the proximal superior sagittal sinus, this area was not studied. The sinuses were examined after the brain was removed from the calvaria by incising the superior surface of the transverse and sigmoid sinuses and the inferior surface of the straight sinus. These incision lines were followed into the sinus confluence. The walls of the dural sinus were examined after they were rinsed with water and preservative solution to remove any postmortem clot. The location, size, morphology, and intrasinus position of the focal protrusions were recorded.

Histologic evaluation was done on eight protuberances in the sinus lumen. Tissues were fixed in formalin and embedded in paraffin. Sections were cut at 5 $\mu$m and stained with hematoxylin-eosin, trichrome, and Verhoeff stains.

## Results

### CT Studies

Discrete filling defects were identified in 138 (24%) of the contrast-enhanced CT examinations. A total of 168 filling defects were identi-
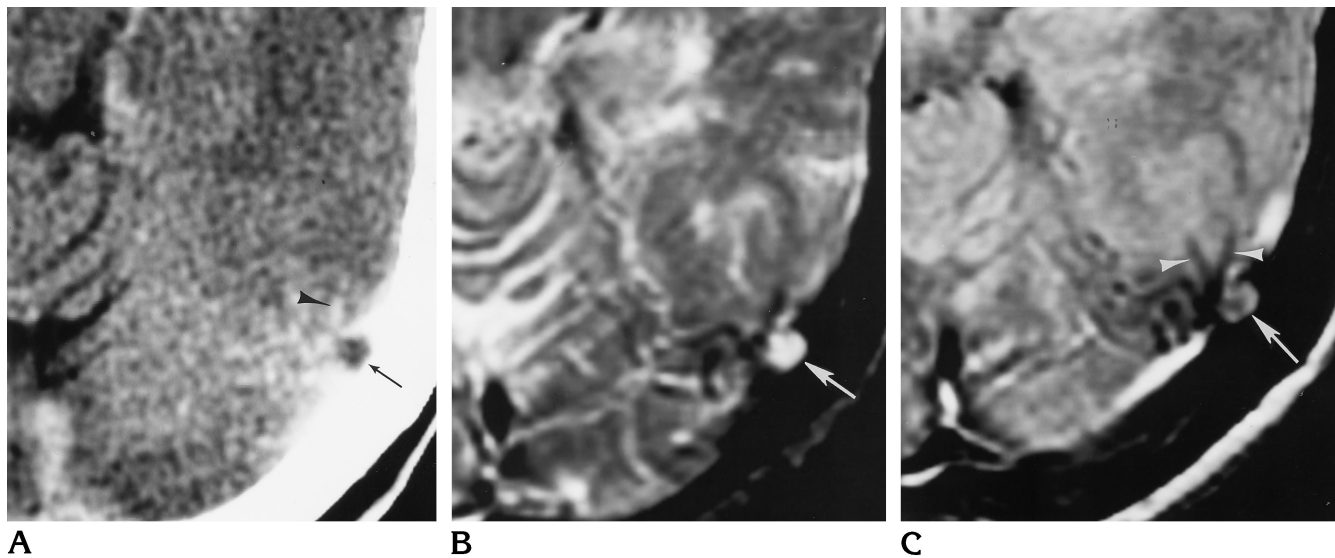
A          B          C

Fig 1. Sixty-two-year-old woman being evaluated for headaches.

*A*, Contrast-enhanced CT scan shows focal filling defect within the lateral left transverse sinus (*arrow*). Note adjacent entering veins (*arrowhead*).

*B*, T2-weighted (2500/90) MR image at the same level shows that the focal filling defect seen in *A* is homogeneously hyperintense and projects into the sinus lumen (*arrow*).

*C*, In this balanced (2500/30) MR image at the same level, the filling defect (*arrow*) exhibits a peripheral hyperintense rim and a central hypointense region. Note the adjacent entering veins (*arrowheads*).

fied in the 138 cases (Table 1). The majority of the defects (92%) were seen within the transverse sinuses, particularly within the middle and lateral portions of the sinus (Figs 1A and 2A). A slight trend toward a left-sided predominance was noted. Eight defects (5%) were identified in the region of the torcular Herophili (dural venous sinus confluence), two (1%) were seen within the straight sinus, and two (1%) were in the sigmoid sinus. In one case, a large defect was present within the distal superior sagittal sinus. (Fig 3A).

Fifty-six (33%) of the defects appeared isodense and 112 (67%) appeared hypodense relative to brain parenchyma on postcontrast imaging studies. Precontrast images were available for 84 defects. Of these, 34 (40%) could be identified as hypodense relative to the slight hyperdensity of blood within the sinuses. No filling defect appeared hyperdense. Multiple filling defects were identified in 19 cases (14% of the cases with filling defects, 3% of all the cases evaluated) (Fig 4). Two defects were seen in 15 cases, and three, four, five, and nine defects were seen in one case each. Filling defects within the transverse sinus were commonly located adjacent to the sites of venous entry (vein of Labbé, cerebellar veins) (95 [62%] of the 154 defects within the transverse

sinus) (Figs 1 and 2). All of these defects were located in the middle to lateral transverse sinus or transverse sinus–sigmoid sinus junction.

The mean size of the defects was 4.0 ± 1.9 mm base dimension (range, 1.3 to 15.0 mm) and 4.2 ± 1.8 mm intraluminal dimension (range, 1.3 to 9.4 mm). The linear distance from the center of the torcular Herophili to the edge of the filling defect was measured for defects within the transverse and sigmoid sinuses. The mean distance was 43.8 ± 11.4 mm (range, 7.7 to 64.1 mm). One hundred twenty-eight defects (82% of the defects in the transverse and sigmoid sinus) were located 40 mm or more from the torcular Herophili.

No difference in sex distribution was noted between the patients with filling defects and those without. As a group, patients in whom filling defects were identified were older than patients who had no filling defects. The mean age of the group with defects was 46 ± 20 years (range, 10 months to 86 years), whereas the mean age of the group with no defects was 40 years ± 21 years (range, 1 month to 92 years) ($P = .005$, Student's two-tailed $t$ test). In those without filling defects, 15% were less than 15 years old and 13% were older than 65, compared with 6% and 24% of cases, respectively, in those who had filling defects (Table 2). The
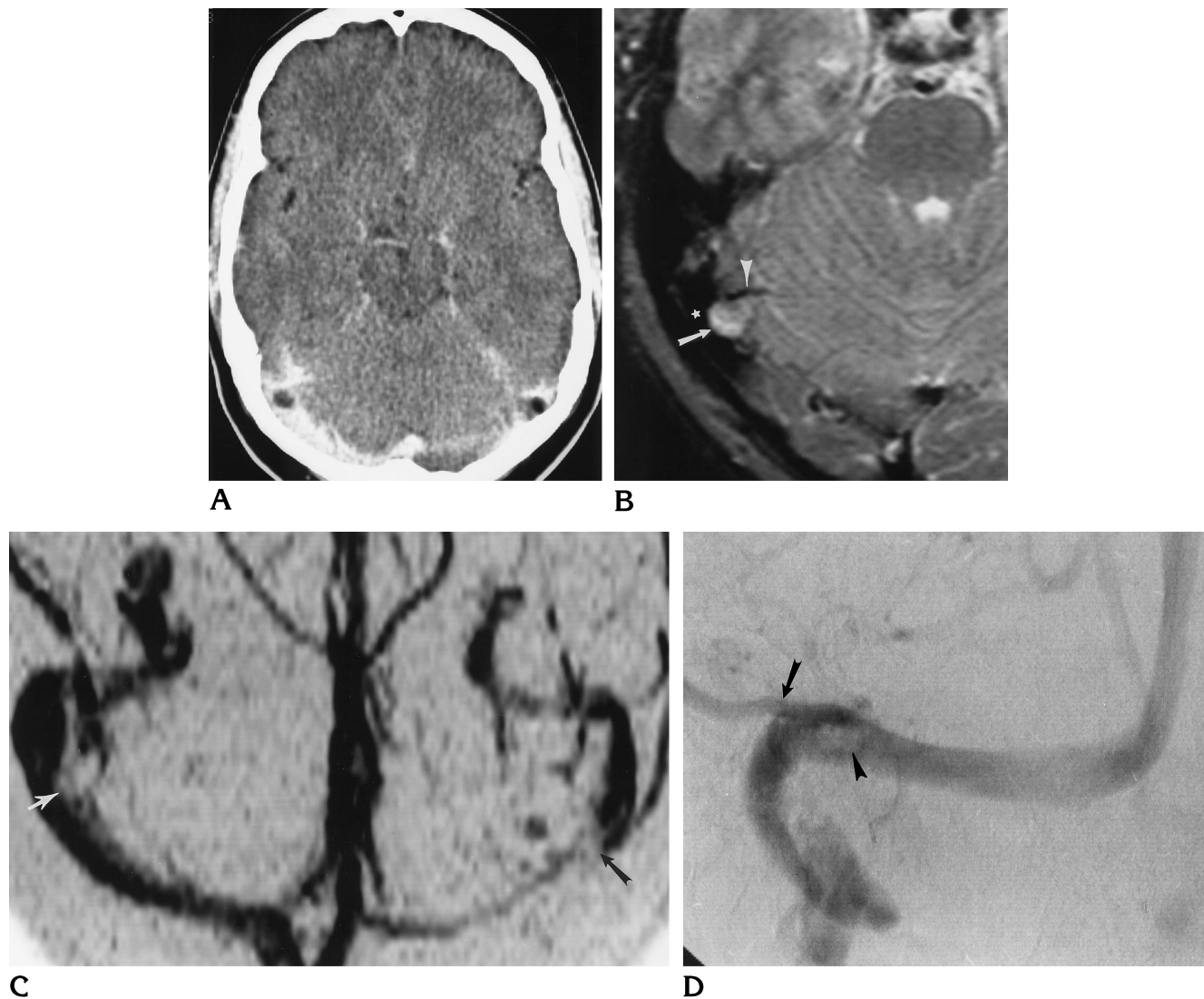
Fig 2. Twenty-nine-year-old man with a several-month history of occipital headaches with frontal radiation.

*A*, Contrast-enhanced CT scan of the head shows round, well-defined filling defects within the lateral aspect of both transverse sinuses, measuring 8 mm. The tentative diagnosis of bilateral transverse sinus thrombosis was made, and we were consulted to perform intrasinus thrombolysis. Because of the atypical appearance of these areas for thrombosis, further imaging was performed for confirmation.

*B*, On this axial T2-weighted (2500/90) MR image, the filling defect is heterogeneously hyperintense (*arrow*) and protrudes into the sinus lumen (*star*). Similar findings were seen in the left transverse sinus. Note the adjacent entering vein (*arrowhead*).

*C*, Two-dimensional time-of-flight MR venogram shows no evidence of thrombosis. The right transverse sinus was dominant and the left proximal transverse sinus partially atretic. Focal defects in the sinus lumen (*arrows*) were noted in the same locations as on the MR and CT studies.

*D*, Venous phase from right carotid digital subtraction angiography. A focal filling defect (*arrowhead*) is seen in the same location as on CT, MR imaging, and MR venographic studies. Note the close relationship of the vein of Labbé (*arrow*).

prevalence of filling defects showed a general tendency to increase with age; 38% of patients older than 65 years had filling defects.

MR images were available for review in 31 of the 138 positive cases identified on CT scans. The MR findings agreed (in location and number of filling defects) in 23 cases (74%). In most cases, the filling defects were not as well delin-eated on MR images. Smaller defects were more easily appreciated on contrast-enhanced CT scans.

## MR Imaging Studies

Focal, well-defined areas of nonflow signal protruding into the sinus lumen, producing de-
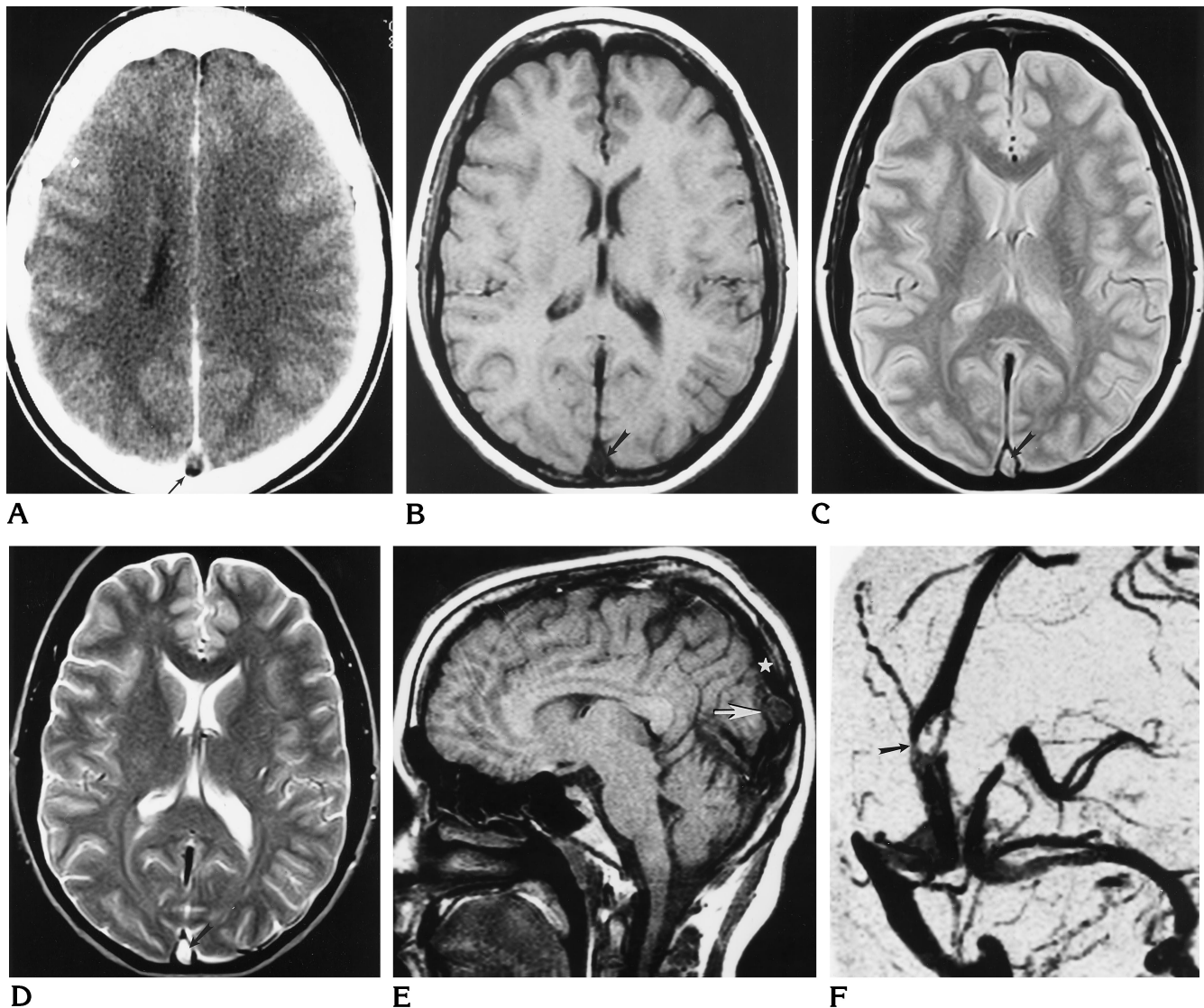
Fig 3. Thirty-two-year-old woman with 5-week history of headaches.

*A,* Contrast-enhanced CT scan shows a focal hypodense mass within the distal superior sagittal sinus (*arrow*). Normal contrast opacification of the sinus was noted on adjacent images.

*B,* Axial T1-weighted (600/10) MR image shows hypointense mass within the distal superior sagittal sinus at the same location (*arrow*).

*C,* On axial balanced (2500/30) MR image at the same level, the mass is heterogeneously hyperintense (*arrow*).

*D,* Axial T2-weighted (2500/90) MR image at the same level shows the mass to be homogeneously hyperintense and occupying almost the entire sinus lumen (*arrow*).

*E,* Sagittal (600/10) T1-weighted MR image shows the focal mass is hypointense with some strandy areas of isointensity (*arrow*) projecting into the sinus lumen (*star*). The inner table of the calvaria is impressed smoothly.

*F,* Projected two-dimensional time-of-flight MR venogram shows a focal filling defect within the sinus lumen (*arrow*), with normal flow noted both proximally and distally.

fects in the contrast column, were identified in 13 (13%) of the 100 randomly selected contrast-enhanced MR examinations. A total of 14 intrasinus foci were identified. Twelve were located in the middle to lateral transverse sinus, one was located in the transverse sinus–sigmoid sinus junction, and one was located in the su-perior sagittal sinus. Of the 13 defects seen in the transverse sinus, 11 (85%) were directly adjacent to vein entry sites. The foci exhibited isointense to hypointense signal relative to brain parenchyma on T1-weighted images (12 were hypointense, one was isointense) (Fig 3B and E), and hyperintense signal on T2-weighted im-
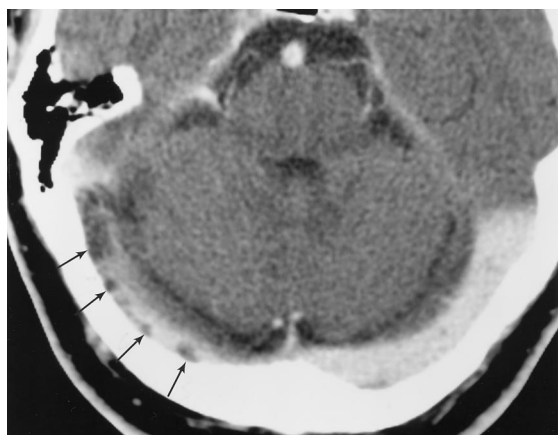
Fig 4. Seventy-three-year-old man with gradual loss of visual acuity (subsequently found to be secondary to cataracts). Contrast-enhanced CT scan shows multiple hypodense foci throughout the right transverse sinus (*arrows*).

TABLE 2: Age distributions of patients with and without focal filling defects within the dural sinuses seen on contrast-enhanced CT examinations

| Age Range of Groups | Percentage (No.) of Age Group with Filling Defects | No. (%) of 138 Cases with Filling Defects | No. (%) of 435 Cases with No Filling Defect |
|---|---|---|---|
| 0–1 y | 22 (2/9) | 2 (1) | 7 (2) |
| >1–15 y | 9 (6/64) | 6 (4) | 58 (13) |
| >15–45 y | 24 (65/266) | 65 (47) | 201 (46) |
| >45–65 y | 22 (32/146) | 32 (23) | 114 (26) |
| >65 y | 38 (33/88) | 33 (24) | 55 (13) |

ages (Figs 1B, 2B, and 3D). The foci were more variable in signal on proton density–weighted images (Figs 1C and 3C). Three were hypointense, six were hyperintense, two were isointense, and three were hyperintense peripherally, with a hypointense center (Fig 1C). No contrast enhancement was identified in any case. The focal defects were seen best on the T2-weighted images, but could be confirmed on all pulse sequences and imaging planes. The mean size of the foci was 5.2 ± 2.3 mm base dimension (range, 2 to 10 mm) and 5.3 ± 2.3 intraluminal dimension (range, 3 to 10 mm). The mean linear distance from midline (transverse sinus foci) was 40 ± 8.2 mm (range, 23 to 55 mm). The defects appeared as focal impressions into the sinus lumen, with surrounding flow signal on MR venograms (Figs 2C and 3F).

## Anatomic Correlation

Lobular protrusions into the dural sinuses were noted in 19 (66%) of 29 cases. A total of

TABLE 3: Location of 91 lobular protrusions into the dural sinuses in 29 cadaveric specimens

| Defect Location | n (%) |
|---|---|
| Right transverse sinus | 25 (27) |
|   Transverse/sigmoid junction | 2 (2) |
|   Midlateral transverse | 19 (21) |
|   Medial transverse near torcula | 4 (4) |
| Left transverse sinus | 61 (67) |
|   Transverse/sigmoid junction | 7 (8) |
|   Midlateral transverse | 53 (58) |
|   Medial transverse near torcula | 1 (1) |
| Torcular Herophili | 5 (6) |

91 focal protuberances were identified (Table 3). The protuberances were spherical to finger-like in shape, and smooth to lobular in contour. Some protuberances had smooth surfaces, others were more irregular (Fig 5A). Sizes ranged from less than 1 mm to 8 mm in diameter (mean, 2.0 mm). The distribution of granulations closely matched the distribution of filling defects seen on contrast-enhanced CT and MR studies. The majority were identified within the transverse sinuses (95%), with 61 (67%) found in the left transverse sinus and 25 (27%) found in the right transverse sinus. Five (6%) were found in the torcular Herophili. No protuberances were identified within the straight sinus, sigmoid sinuses, or distal superior sagittal sinus. Most of the protuberances within the transverse sinus projected from the anterior inferior aspect of the sinus directly into the sinus lumen. As on imaging, the protuberances were often closely associated with cortical venous entrance sites into the sinus (Fig 5A).

On microscopic evaluation, the protuberant masses were composed of a mixture of variably dense fibrous connective tissue containing numerous fibroblasts, scattered arachnoid cell nests, and an irregular network of small vessels and delicate endothelium-lined spaces, most prominent in the basal regions (Fig 5B). Trabeculated channels with attenuated endothelial lining were often seen in the core of the granulations. The protuberances projected through the portion of the dura comprising the sinus walls and into the lumen, where the structure was covered by an endothelial cell layer continuous with the sinus lining. Proximity to venous entrance sites was again noted, as seen on gross examination.

Smaller granulations exhibited a characteristic architecture with an irregular, loose fibrous connective tissue core and a more peripheral, dense,
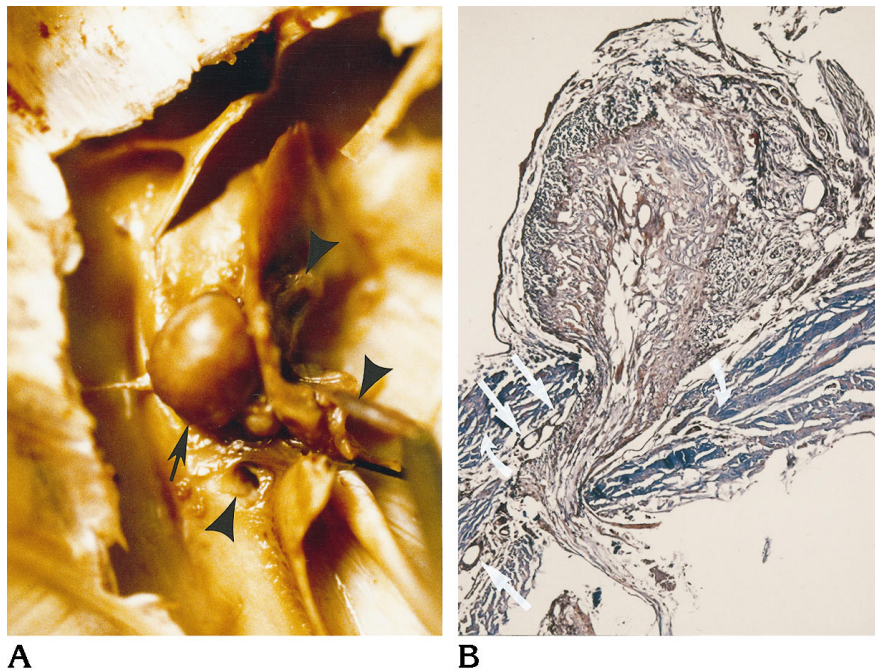
**A** **B**

Fig 5. Correlative anatomic specimens.

A, Superior view of gross specimen of the left lateral transverse sinus near the transverse sinus–sigmoid sinus junction. The superior sinus wall has been removed. A 8-mm focal protuberance into the sinus lumen is seen projecting from the anterior sinus wall (*arrow*). The protuberance has a smooth surface and is closely associated with entering veins (*arrowheads*).

B, Light microscopic study of a typical arachnoid granulation shows central core of loose and peripheral zone of dense connective tissue projecting through the dura of the sinus wall (*curved arrows*). Adjacent venous structures are seen at the granulation base (*straight arrows*). Endothelium continuous with the endothelial covering of the sinus lumen is seen on the surface of the granulation (trichrome stain, original magnification ×16).

hyalinized connective tissue layer. Most small granulations exhibited a simple, smooth surface contour. The larger granulations were more complex and contained an admixture of both dense and loose connective tissue within the core. The gross and microscopic appearance of these structures compare closely with previous descriptions of arachnoid granulations (13, 14).

## Discussion

We have shown that focal filling defects are present in the dural sinuses in 24% of randomly selected contrast-enhanced CT examinations. These defects are well circumscribed, hypodense to isodense relative to brain parenchyma, and predominantly located in the lateral transverse sinuses. Comparison with MR findings showed the defects to be hypointense on T1-weighted images, variable in signal on proton density–weighted images, and hyperintense on T2-weighted images. Randomly selected MR examinations of the brain revealed focal signal alterations in the dural sinuses in 13% of cases, matching the defect distribution seen on CT scans. Although direct anatomic correlation was not possible in our case material, our review of 29 cadaveric specimens revealed arachnoid granulations in 66% of cases in a distribution matching that of the filling defects seen on imaging studies.

It is possible that some of the filling defects seen in our study could have been caused by processes other than arachnoid granulations. Intrasinus septa, venous sinus duplications (7), partial volume averaging of adjacent brain or dura, or normal variations in sinus contrast density on CT scans (with delayed scanning) (8) could all produce relative defects or signal alterations within the dural sinuses. The focal distribution, well-defined morphology, and circumferential contrast around the defects seen in this study makes these possibilities unlikely. All the evaluated contrast-enhanced CT scans in this study were obtained immediately after bolus contrast administration and during drip contrast infusion.

Inflow of unopacified blood can produce apparent intrasinus filling defects on angiograms (22); however, these defects would not be expected on contrast-enhanced CT or MR examinations. Slow or turbulent flow can cause unusual signal within the dural sinuses on MR images (4); however, these signals are rarely focal and would not be present on contrast-enhanced CT scans in the same location, as they were in many of our cases.

Arachnoid granulations are normally occurring focal protuberances of the leptomeninges into the dural venous sinus lumen (13, 16). Arachnoid granulations and arachnoid villi differ primarily in size and complexity of structure. Arachnoid granulations are visible to the unaided eye, whereas arachnoid villi are microscopic structures (13, 14, 16, 17). Besides be-

ing larger, granulations exhibit more extensive collagenous deposition and hyalinization (14, 18). They are most commonly found within the lacunae laterales of the superior sagittal sinus, although they can also protrude directly into the sinus lumen (14–16). The anatomic distribution of arachnoid granulations in humans has been incompletely studied, but they are thought to be present in the superior sagittal sinus, transverse sinus, cavernous sinus, superior petrosal sinus, and straight sinus in decreasing frequency (15, 16); and they have also been described in relation to spinal veins (19). Arachnoid granulations increase in number and conspicuity with age (10, 14, 16), a finding supported by this imaging study. Arachnoid granulations are commonly found in relation to venous entry sites into the sinus (15, 16, 18–20). This relationship has been described grossly, microscopically, and ultrastructurally (19, 20). Arachnoid granulations adjacent to venous entry sites represent perivascular protrusions of the leptomeninges at regions where the dura mater opens to allow the passage of veins into the dural sinus (19). The distribution of arachnoid granulations in this study also reflects this relationship, with 62% of the transverse sinus arachnoid granulations seen on CT scans and 85% of the transverse sinus granulations seen on MR images directly related to venous entry sites.

Arachnoid granulations exhibit characteristic microscopic features that closely correspond to those found in our cadaveric study (13, 14, 16, 20, 21). Arachnoid granulations are essentially herniations of the arachnoid through the dura wall of a venous sinus. A neck of arachnoid penetrates an aperture in the dura and expands to form the core of the granulation (13). This core is surrounded by a thin cupola of fibrous tissue continuous with the dura. This covering may be intact or fade out near the apex of larger granulations. The core is separated from the dural cupola by the subdural space, which diminishes toward the granulation apex (13, 20). The core is composed of loose fibrous connective tissue forming a trabeculated network with wide interstices and endothelium-lined channels (13, 14, 16, 20). Focal aggregates of arachnoid cells are present along the surface of the core, the so-called arachnoid cell cap (13, 16). As also demonstrated in our study, arachnoid granulations assume a more lobular, complex morphology and become more hyalinized with increasing size (13, 16, 20).

Although described by Pacchioni in 1705 (14), the function of arachnoid granulations is still incompletely understood. They are thought to play a major role in resorption of cerebrospinal fluid, although the exact mechanism is incompletely elucidated. It is likely that a combination of a transendothelial direct tubular system (17, 21), intact membrane filtration (21), and vesicular transport (23) are at play. Although the number of arachnoid villi are much greater than the number of granulations, the relative combination of each to cerebrospinal fluid resorption is unknown (20). Another function attributed to arachnoid granulations is as a potential cerebrospinal fluid volume buffer (19).

There have been few dedicated anatomic studies of arachnoid granulations within the transverse sinuses. Most anatomic studies have evaluated arachnoid granulations within the superior sagittal sinus. Browder et al (18, 24) described 33 smooth-surfaced nodules projecting into the dural sinuses within 32 of 380 cadavers. In their studies, the nodules ranged in size from 3 to 24 mm in maximum dimension; 26 of the 33 were identified within the left transverse sinus. As in our study, the nodules were commonly associated with venous entry sites into the sinus, particularly the vein of Labbé. Two of the 33 nodules were found in the right transverse sinus and two large nodules were seen within the distal superior sagittal sinus. This distribution coincides with our observations on imaging studies and anatomic dissections, with the exception of the more striking left-sided distribution in their study. Our study revealed a higher prevalence of arachnoid granulations, most likely caused by the inclusion of smaller protuberances (mean, 2 mm).

A few reports have described the imaging appearance of arachnoid granulations. Grossman and Potts (10) described their appearance on angiograms and plain radiographs. Impressions in the skull from arachnoid granulations were identified in 46% of 400 randomly selected skull films, increasing in prevalence with age. The majority were found in the anterior parietal region, close to the midline. Angiographically, arachnoid granulations appeared as filling defects within the lacunae laterales (and in one case within the lumen of the superior sagittal sinus), usually closely related to cortical veins. No arachnoid granulation relating to the lumen of the transverse sinus was seen at angiography.

The appearance of arachnoid granulations on contrast-enhanced CT scans was described by Tokiguchi et al (9), who described a 2 × 3-mm hypodense filling defect within the left transverse sinus, similar in appearance to the granulations seen in our study. This was subsequently proved histologically to represent an arachnoid granulation with an appearance that was identical to that in our cases.

Curé et al, in a review of normal dural sinus anatomy (1), described two cases of large filling defects within the superior sagittal sinus and transverse sinus on CT and MR studies. These were hypodense on contrast-enhanced CT scans and hypointense to isointense on T1-weighted MR images. No description of their appearance on T2-weighted MR images or information on contrast enhancement was provided. These also appeared as focal filling defects on MR venograms and standard angiograms. Mamourian and Towfighi (11) described a large arachnoid granulation within the superior sagittal sinus on MR images, MR venograms, and CT scans. The mass was focal, isointense to hypointense on T1-weighted images, hyperintense on T2-weighted images, and showed minimal heterogeneous contrast enhancement. No cases of contrast enhancement were found in our series, even in the largest granulations. The contrast enhancement seen in their study may be related to adjacent intraluminal enhancement or easier identification owing to larger granulation size. They performed a limited autopsy study of 10 cases and found three granulations in two cases. Two were present in the transverse sinuses and one in the superior sagittal sinus. The prevalence of arachnoid granulations in our anatomic study was much greater; again most likely because we identified much smaller granulations (mean size, 2 mm).

Roche and Warner, in a recent imaging study (12), described filling defects identical to those seen in our study and estimated a frequency of occurrence of between 0.3 and 1 in 100 adult patients. Their CT scans were obtained with 3-mm sections at 5-mm intervals through the posterior fossa, instead of the 3-mm or 5-mm contiguous scans used in our study, which probably underestimated the true frequency. They reviewed 200 T1-weighted MR studies obtained with 2-mm adjacent sections through the transverse sinuses and found two granulations. No contrast material was used. As documented in our study, arachnoid granulations are optimally identified on T2-weighted images or on contrast-enhanced T1-weighted images. Arachnoid granulations within the distal superior sagittal sinus, transverse sinuses, and sigmoid sinuses are common, occurring in 66% of cases in our careful anatomic study. The underestimation of the true prevalence on imaging examinations is most likely due to partial volume averaging effects relating to section thickness and section-selection parameters.

Despite the common finding of arachnoid granulations within the superior sagittal sinus in previous anatomic studies (15–17), the vast majority of the filling defects seen on CT or MR examinations in our study and in the literature are present within the transverse sinuses. One reason for this is that most arachnoid granulations in the anterior superior sagittal sinus actually protrude into the lacunae laterales and not into the sinus lumen (10, 14–16). Arachnoid granulations, producing calvarial impressions, occur between 13 and 15 mm lateral to midline in this region (10). These would not present as focal intrasinus filling defects, and would not be confused with thrombosis on imaging studies. The axial imaging plane of the CT examinations in this study affords poor visibility of the proximal superior sagittal sinus, and some defects in this region could have been missed. MR examinations, however, allowed imaging in three planes, and no proximal superior sagittal sinus intraluminal foci were identified.

The CT density of granulations in this study, and in the literature, varied from being like cerebrospinal fluid to being isodense with brain. Despite the potential for psammomatous calcification in arachnoid granulations (12, 14), no calcifications were seen on the CT examinations or anatomic specimens in our study. MR signal intensity is more variable; however, almost all granulations appeared hyperintense on long-repetition-time/echo-time sequences. The variable CT density and MR signal intensity most likely represents the variable amounts of connective tissue and cerebrospinal fluid within the granulation as well as partial volume effects from the adjacent contrast-filled dural sinus.

Arachnoid granulations can be easily distinguished from thrombosis. Thrombosis usually involves an entire segment of sinus or multiple sinuses, and can extend into cortical veins (2–5). Arachnoid granulations produce focal, well-defined defects or signal foci. The density and signal of arachnoid granulations are also differ-

ent from those seen with thrombosis. Usually, with acute thrombosis, hyperdensity is seen within the sinus lumen on CT scans, and variable signal intensity (usually T1 hyperintensity) is seen on MR images (depending on the age of the thrombus and the pulse sequence) (2, 4). Arachnoid granulations were never hyperdense or T1-hyperintense in our cases. Abnormal flow is usually seen distal to a thrombosed segment of sinus. Normal sinus contrast opacification on CT scans, flow void on MR images, and intrasinus signal on MR venograms are seen both proximally and distally to arachnoid granulations. The characteristic distribution of arachnoid granulations (lateral transverse sinus associated with venous entrance sites) also helps to identify and differentiate these entities from thrombosis. No secondary signs of thrombosis or venous hypertension (collateral veins, dural enhancement, brain swelling) were noted, even with the largest filling defects.

We have not encountered a case ourselves, or in the literature, in which arachnoid granulations (within the dural sinus) have been solely responsible for a patient's symptoms. Roche and Warner (12) reviewed the clinical history of 32 patients with arachnoid granulations within the transverse sinuses and found no convincing evidence of related symptoms. It stands to reason, however, that large granulations could produce relative luminal compromise and lead to a pressure gradient or disturbed flow. This could lead, in turn, to venous hypertension (if the superior sagittal sinus or dominant transverse sinus were involved) or to thrombosis (if flow were sufficiently slow or in hypercoagulable states).

In summary, focal filling defects within the dural venous sinuses, consistent with arachnoid granulations, are seen on 24% of contrast-enhanced CT scans and on 13% of contrast-enhanced MR examinations of the brain. They are typically located within the transverse sinuses, adjacent to venous entrance sites. They can be differentiated from thrombosis and intrasinus tumor by their characteristic location, well-defined morphology, density, and signal characteristics.

## References

1. Curé JK, Van Tassel P, Smith TM. Normal and variant anatomy of the dural venous sinuses. *Semin Ultrasound CT MR* 1994;15:499–519

2. Curé JK, Van Tassel P. Congenital and acquired abnormalities of the dural venous sinuses. *Semin Ultrasound CT MR* 1994;15:520–539

3. Zouaoui A, Hidden G. Cerebral venous sinuses: anatomical variants or thrombosis? *Acta Anat (Basel)* 1988;133:318–324

4. Zimmerman RD, Ernst RJ. Neuroimaging of cerebral venous thrombosis. *Neuroimaging Clin N Am* 1992;2:463–485

5. Buonanno FS, Moody DM, Ball MR, et al. Computed cranial tomographic findings in cerebral sinovenous occlusion. *J Comput Assist Tomogr* 1978;2:281–290

6. Harris TM, Smith RR, Koch JK. Gadolinium-DTPA enhanced MR imaging of septic dural sinus thrombosis. *J Comput Assist Tomogr* 1992;16:25–29

7. Huang YP, Ohta T, Okudera T, et al. Anatomic variations of the dural sinuses. In: Kapp JP, Schimidek HH, eds. *The Cerebral Venous System and Its Disorders*. Philadelphia, Pa: Grune & Stratton; 1984:109–167

8. Ulmer JL, Elster AD. Physiologic mechanisms underlying the delayed delta sign. *AJNR Am J Neuroradiol* 1991;12:647–650

9. Tokiguchi S, Hayashi S, Takahashi H, et al. CT of the pacchionian body. *Neuroradiology* 1993;35:347–348

10. Grossman CB, Potts DG. Arachnoid granulations: radiology and anatomy. *Radiology* 1974;113:95–100

11. Mamourian AC, Towfighi J. MR of giant arachnoid granulations: a normal variant presenting as a mass within the dural venous sinus. *AJNR Am J Neuroradiol* 1995;16:901–904

12. Roche J, Warner D. Arachnoid granulations in the transverse and sigmoid sinuses: CT, MR, and MR angiographic appearance of a normal anatomic variation. *AJNR Am J Neuroradiol* 1996;17:677–683

13. Wolpow ER, Schaumberg HH. Structure of the human arachnoid granulation. *J Neurosurg* 1972;37:724–727

14. Turner L. The structure of arachnoid granulations with observations on their physiologic and pathological significance. *Ann R Coll Surg Engl* 1961;29:237–264

15. Key A, Retzius G. *Stadien in der Anatomie des Nerven systems und des Bind egenwebes*. Stockholm, Sweden: Norstedt and Soner; 1876;2

16. LeGros Clark WE. On the pacchionian bodies. *J Anat* 1920;55:40–48

17. Potts DG, Reilly K, Deonaner V. Morphology of the arachnoid villi and granulations. *Radiology* 1972;105:333–341

18. Browder J, Kaplan H, Howard J. Hyperplasia of pacchionian granulations. *Arch Pathol* 1973;95:315–317

19. Krisch B. Ultrastructure of the meninges at the site of penetration of veins through the dura mater, with particular reference to pacchionian granulations: investigations in the rat and two species of New-World monkeys (*Cebus apella, Callitrix jacchus*). *Cell Tissue Res* 1988;251:621–631

20. Upton ML, Weller RO. The morphology of cerebrospinal fluid drainage pathways in human arachnoid granulations. *J Neurosurg* 1985;63:867–875

21. Gomez DG, Potts DG. The surface characteristics of arachnoid granulations: a scanning electron microscopical study. *Arch Neurol* 1974;31:88–93

22. Hacker H. Normal supratentorial veins and dural sinuses. In: Newton TH, Potts DG, eds. *Radiology of the Skull and Brain*. St Louis, Mo: Mosby; 1974;2(3):1869

23. Tripathi BJ, Tripathi RC. Vacuolar transcellular channels as a drainage pathway for cerebrospinal fluid. *J Physiol (Lond)* 1974;239:195–206

24. Browder J, Browder A, Kaplan K. Benign tumors of the cerebral dural sinuses. *J Neurosurg* 1972;37:576–580